ceramics

MDPI

Article

Thermally Activated $Al(OH)_3$ Part II—Effect of Different Thermal Treatments

Bogdan Stefan Vasile [1,2,3,*], Gheorghe Dobra [4], Sorin Iliev [5], Lucian Cotet [5], Ionela Andreea Neacsu [1,2,3], Vasile Adrian Surdu [1,2,3], Adrian Ionut Nicoara [1,2,3], Alina Boiangiu [5] and Laurențiu Filipescu [1]

1 Faculty of Applied Chemistry and Materials Science, University Politehnica of Bucharest, 060042 Bucharest, Romania; neacsu.a.ionela@gmail.com (I.A.N.); adrian.surdu@upb.ro (V.A.S.); adi.nicoara18@gmail.com (A.I.N.); laurentiu_filipescu@yahoo.co.uk (L.F.)
2 National Research Center for Micro and Nanomaterials, University Politehnica of Bucharest, 060042 Bucharest, Romania
3 Academy of Romanian Scientists, Ilfov Str. No. 3, 50044 Bucharest, Romania
4 Alro Slatina SA, Pitesti Street, no. 116, 230048 Slatina, Romania; dobra@alro.ro
5 Alum Tulcea SA, Isaccei Street, no. 82, 820228 Tulcea, Romania; siliev@alum.ro (S.I.); lcotet@alum.ro (L.C.); aboiangiu@alum.ro (A.B.)
* Correspondence: bogdan.vasile@upb.ro

Abstract: In this paper, the thermal decomposition of crystalline $Al(OH)_3$ was studied over the temperature range of 260–400 °C for particles with a size between 10 and 150 µm. The weight losses and thermal effects occurring in each of the dehydration process were assessed using thermogravimetry (TG) and differential scanning calorimetry (DSC) thermal analysis. X-ray diffraction (XRD) patterns, refined by the Rietveld method, were used for mineral phase identification, phase composition analysis, and crystallinity degree determination. Moreover, the particle size distributions and their corresponding D10, D50, and D90 numeric values were determined with a laser analyzer. We observed a strong relationship between the calcination temperature, the initial gibbsite grade particle size, and the crystallinity of the resulting powders. Hence, for all endothermic effects identified by DSC, the associated temperature values significantly decreased insofar as the particle dimensions decreased. When the gibbsite was calcined at a low temperature, we identified small amounts of boehmite phase along with amorphous new phases and unconverted gibbsite, while the powders calcined at 400 °C gradually yielded a mixture of boehmite and crystalized γ-Al_2O_3. The crystallinity % of all phase transition products declined with the increase in particle size or temperature for all the samples.

Keywords: aluminum hydroxide; alumina; thermal treatment; crystallinity

Citation: Vasile, B.S.; Dobra, G.; Iliev, S.; Cotet, L.; Neacsu, I.A.; Surdu, V.A.; Nicoara, A.I.; Boiangiu, A.; Filipescu, L. Thermally Activated $Al(OH)_3$ Part II—Effect of Different Thermal Treatments. *Ceramics* **2021**, *4*, 564–575. https://doi.org/10.3390/ceramics4040040

Academic Editor: Gilbert Fantozzi

Received: 16 June 2021
Accepted: 8 October 2021
Published: 11 October 2021

1. Introduction

Alumina (Al_2O_3) and its partial hydrates prove to be extremely valuable materials in many practical applications, usually as desiccants [1–3], fillers [4–6], adsorbents [7–10] for the removal of oil and grease from industrial waters [11], organic powder coatings [12–14], porous ceramics [15–17], high-temperature ceramic oxides [18–20], ceramic filtration membranes [21–24], and catalysts [25–29], only if the precursors are properly prepared and thermally treated [30–32]. Among the desired properties for these applications are a specific pore size and pore size distribution [33,34], a high specific surface area [35–37], and the degree of crystallinity, which also plays an essential role [38–41]. When discussing the synthesis routes for α-Al_2O_3, the thermal transformation of aluminum oxy-hydroxides remains the most studied [42].

Gibbsite ($Al(OH)_3$), a natural aluminum trihydrate, is a component of bauxites, beside boehmite (AlOOH), and diaspore (AlO_2H), and without any doubt, as an industrial product, is the only one manufactured at an industrial scale among all the hydrated aluminas. Diaspore is a remarkable product because it is the only aluminum oxy-hydroxide that

can be easily and directly dehydrated to α-alumina due to its structural resemblances to α-Al_2O_3 (a hexagonal close-packed structure). The transformation of boehmite to diaspore is possible only if very high pressures are applied [43]. Boehmite is an aluminum oxyhydroxide with important applications in its natural state or as a precursor for different materials used in catalysis and adsorption processes. The most known research target in the low-temperature alumina domain is growth promotion of the γ-Al_2O_3 phase [44,45]. Gibbsite $Al(OH)_3$ is industrially produced by Bayer's process and its final particle size and morphology are strongly influenced by the process parameters [46,47]. Normally, gibbsite is fully transformed into α-alumina at 1100–1300 °C. This high calcination temperature leads to large crystallites with peculiar grain growth and to a decrease in density associated with poor mechanical properties for the sintering of ceramic bodies [48]. It is therefore necessary to reduce the calcination temperature and several studies suggest doing this by reducing the initial gibbsite particles' size [49,50]. Jang et al. [50] concluded that milling the gibbsite for 8 h leads to a transformation temperature of 1000 °C, while Tsuchida and Ichikawa [51] achieved this transformation at a temperature of 1100 °C after 30 min of mechano-chemical activation. For instance, Kano et al. [52] reported a temperature reduction from 1350 to 1020 °C by grinding the gibbsite powder for 60 min, with no additional improvements if the grinding time is extended. This effect is expected to happen also when the gibbsite is calcined at a lower temperature to obtain the transition aluminas as precursors. The successive decomposition of gibbsite, after the thermal treatment, did yield combinations of different compounds, the most common being boehmite and/or transition alumina phases (including χ, κ, γ, δ, θ, and η), that were more or less amorphous [38,41]. From a structural point of view, these intermediary products have the aluminum atoms surrounded by oxygen atoms in a tetrahedral and octahedral structure. The ratio between the AlO_6 units (characteristic of octahedral coordinated α-Al_2O_3) and the AlO_4 units (characteristic of tetrahedral coordinated transitional alumina) changes for different polymorph phases, which ultimately modifies their properties, including the crystal packing, electronic structure, and dielectric constant [32,35]. Important aspects of the gibbsite dehydration process and the corresponding transition phases have been studied for years at various heating rates. After extensive research, the literature reports unanimously indicate the order in which the compounds are formed during the thermal transformation, but not the kinetics of the dehydration processes or their associated mechanisms [53].

When a higher heating rate is applied, the fine gibbsite particles are partially transformed into an amorphous product (ρ-alumina) with increased reactivity and thermal stability until 800 °C [32]. In particular, when the heating rate is in accordance with the equilibrium conditions, the dehydration and the crystal lattice transformation happen to take place at the same time, resulting in crystalline oxidic compounds (boehmite at temperatures higher than $T > 180$ °C and χ-Al_2O_3 at $T \geq 250$ °C) [37].

The purpose of this paper is to investigate the physical, chemical, and mechanical properties of a specific aluminum hydroxide material produced by a specific technology (a Bayer-modified technology), finished off through drying, milling, and classification, and ultimately calcined at low temperatures in order to produce low-temperature aluminas. The selection of the properties to be evaluated was made because of the disputable quality of the raw material in terms of granulometry and purity. Thus, the thermally treated products from this raw material might find applications in domains such as fillers, adsorbents in heavily polluted industrial water, oil and grease removal from industrial waters, organic powder coatings, extenders in other types of coating materials, and fire retardants. Additionally, to improve the quality of the thermally treated materials, the temperature and time of treatment were selected in such a way to promote the emergence of amorphous phases.

According to the literature, each industrial aluminum hydroxide grade has similar properties to the other grades, but also certain specific properties. Thus, during grinding, heating, and other thermal or non-thermal treatments, the final products differ mainly in terms of phase composition and properties. Hence, the thermal decomposition of

crystalline $Al(OH)_3$ was studied for particle dimension classes between 10 and 150 μm at the following temperature values: 260 °C, 300 °C, and 400 °C. Actually, these temperature values were placed in the phase transition interval as follows: 260 °C at the beginning of the transition gibbsite–boehmite; 300 °C close to the end of the transition gibbsite–boehmite; and 400 °C at the beginning of the transition boehmite–γ alumina.

When the principal properties of these low-temperature aluminas are well known, the accumulated data will help us to determine the destinations of each product: a commercial product, a precursor, or a raw material for another product with a particular use.

2. Materials and Methods

2.1. Sample Preparation

Various samples of aluminum hydroxide powders were received from SC ALUM SA. These samples were produced by Bayer's process and further collected from the newly built line for the production of special grades of dried, milled, and classified aluminum hydroxide that was recently presented by Dobra et al. [47]. In order to study the thermal transformations, the received powders were firstly dried at 60 °C for 24 h, and then heated in an electric furnace (in an air atmosphere) at 260 °C, 300 °C, and 400 °C for 2 h with a heating rate of 5 °C/min. The samples were afterwards slowly cooled in the oven until they reached room temperature. The choice of heating temperature in the thermal treatment was based on literature data concerning the aluminum hydroxide's activation by advanced grinding, and eventually on expected changes in the phase transition mechanism and amorphization rate. More information regarding their classification and calcination can be found in Table 1.

Table 1. Samples of dried, milled, and thermally treated aluminum hydroxide classified by particle size dimension.

Sample Code	Dimensions after Milling	Calcination Temperature (°C)
GDAH-02	<45 μm = 98.29%	-
GDAH-02-260	<45 μm = 98.29%	260
GDAH-02-300	<45 μm = 98.29%	300
GDAH-02-400	<45 μm = 98.29%	400
GDAH-03	<20 μm = 92.13%	-
GDAH-03-260	<20 μm = 92.13%	260
GDAH-03-300	<20 μm = 92.13%	300
GDAH-03-400	<20 μm = 92.13%	400
GDAH-04	<10 μm = 76.28%	-
GDAH-04-260	<10 μm = 76.28%	260
GDAH-04-300	<10 μm = 76.28%	300
GDAH-04-400	<10 μm = 76.28%	400
GDAH-05	<45 μm = 0.001%; >150 μm = 6.54%	-
GDAH-05-260	<45 μm = 0.001%; >150 μm = 6.54%	260
GDAH-05-300	<45 μm = 0.001%; >150 μm = 6.54%	300
GDAH-05-400	<45 μm = 0.001%; >150 μm = 6.54%	400

2.2. Characterization Methods

The kinetics parameters of the thermal transformations studied in this paper were measured by recording the weight losses and thermal effects occurring during the various dehydration processes on a STA 449 F3 Jupiter device (NETZSCH-Gerätebau GmbH, Selb, Germany). The samples were heated at a constant rate of 10 °C/min from room temperature to 1000 °C in a dynamic atmosphere of air with a flow rate of 50 mL/min.

The phase analysis studies by X-ray diffraction (XRD) were carried out using a PANalytical Empyrean diffractometer (Almelo, Netherlands) at room temperature with a characteristic Cu X-ray tube (λ Cu $K_{\alpha 1}$ = 1.541874 Å), in-line focusing, a programmable divergent slit on the incident side, and a programmable anti-scatter slit mounted on the PIXcel3D detector on the diffracted side. The samples were scanned in a Bragg–Brentano geometry

with a scan step increment of 0.02° and a counting time of 255 s/step. The XRD patterns were recorded in the 2θ angle range of 5–90°. The crystallinity and phase composition were refined by the Rietveld method using the HighScore Plus 3.0e software.

Particle size distributions in the analyzed samples were determined using a Malvern Panalytical Mastersizer 2000 diffraction analyzer (Almelo, The Netherlands) in the dynamic range of 0.1 to 3000 μm. Samples were dispersed in water using ultrasound and mechanical stirring. The Mie scattering theory specific to the instrument's software was used for the particle size distribution assessment.

3. Results and Discussion

Differential scanning calorimetry (DSC), thermogravimetry (TG), and X-ray diffraction (XRD) are essential tools in determining the kinetics parameters for all phase transitions of gibbsite. Figure 1 shows the TG and DSC curves of aluminum hydroxide powders heated up to 1000 °C at a heating rate of 10 °C/min. The first decomposition/transition step, between 215 and 260 °C, is best observed for the GDAH-05 sample (minimum at 231 °C) and can be attributed to the partial dehydroxylation of $Al(OH)_3$ accompanied by a mass loss of up to ~5.63% (which is about one molecule of water for four units of $Al(OH)_3$). This reaction was hardly observed in the DSC patterns of the fine-grained gibbsite samples. The corresponding endothermic effects are visible at 231 °C (for GDAH-03 and GDAH-04), 231.4 °C (for GDAH-05), and 234.7 °C (for GDAH-02) but they take place with an insignificant loss of water. For sample GDAH-05, this first transition process was quickly followed by the second decomposition/transition step, between 260 and 320 °C, with a 20.51% mass loss at 306.2 °C. For the samples containing fine particles (after milling), this second endothermic effect has a much higher intensity, covers the first one almost entirely, and is associated with a mass loss of 26–27%. This step has a minimum point between 292.9 °C and 306.2 °C in all samples and again can be attributed to gibbsite dehydroxylation, with AlOOH most probably the final product. The results are in good agreement with literature data, which indicate two concurrently occurring processes at this stage, namely the formation of boehmite and the transformation of gibbsite in some amorphous or χ-Al_2O_3 phase [41,42]. The boehmite will undergo transformation to γ-Al_2O_3 above 320 °C. The main endothermic effect for this process was observed at around 500 °C. The final product represents ~64% of the initial mass for all the samples.

Each chemical and phase transformation that generates the overlapping endothermic effects is firmly influenced by the experimental parameters, such as heating rate, water vapor pressure, and particle dimension. It is easy to observe a connection between the temperature at which the decomposition steps occur and the initial gibbsite particle size. Hence, for all identified endothermic effects, the associated phase transition temperatures considerably decreased when the particle sizes were significantly diminished. For instance, the GDAH-04 product, 76.28% of whose particles are <10 μm in size, decomposed to form transition aluminas at 484.4 °C. In comparison, the GDAH-05 product, whose particles are mostly between 45 and 100 μm in size, displayed the same effect at 519.1 °C.

Similar results were first reported by Brown et al. [54], who identified a combination of boehmite and transition aluminas as decomposition/transition products of large-grained $Al(OH)_3$ particles by observing distinct peaks for each transformation in different thermal analyses (DTA and DSC). These results were further acknowledged by Yamaguchi and Sakamoto [55], who demonstrated that the resulting boehmite was the product of an in situ dissolution process of $Al(OH)_3$ followed by the recrystallization of AlOOH, a theory later confirmed by several studies [56,57]. The rate of this internal dissolution process proved to be highly dependent on the $Al(OH)_3$ particle size, since larger particles have an enhanced ability to retain a higher volume of water and thus facilitate boehmite formation [58].

All these transformations of gibbsite and the chemical composition of the calcined samples were confirmed by the XRD analysis as shown in Figure 2 and Table 2. For the dried sample without the thermal treatment, or samples calcined at a low temperature, gibbsite was the main mineralogical phase identified (ICDD PDF4+ [01-080-6432]), while

for the samples calcined at 400 °C a mixture of boehmite (ICDD PDF4+ [04-010-5683]) and crystalized γ-Al_2O_3 (ICDD PDF4+ [04-005-4662]) was also formed. There were no X-ray peaks associated with the other polymorphic phases of alumina identified at this stage. However, some amorphous phases with variable concentrations in the phase mixtures were found in all samples. The results are in accordance with literature studies [41,59,60].

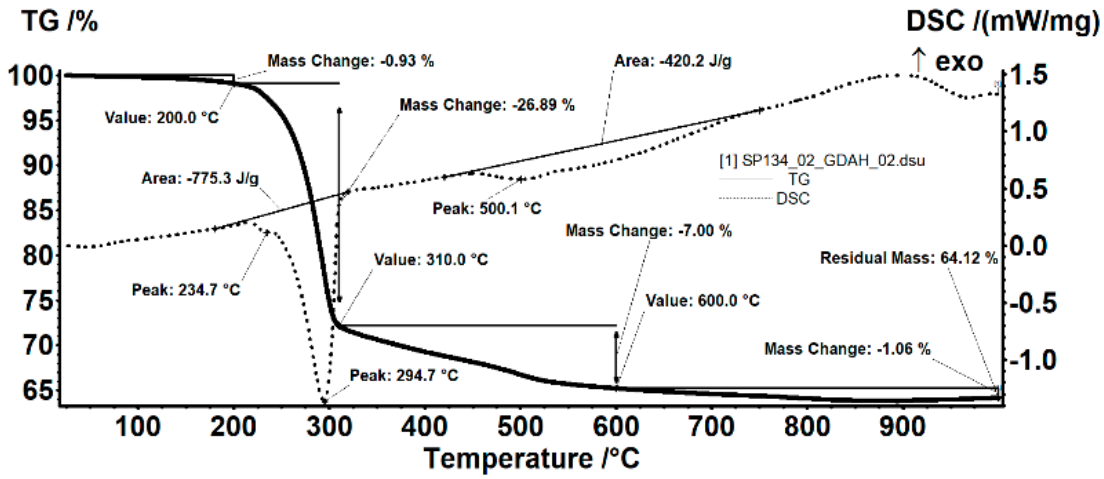

GDAH-02

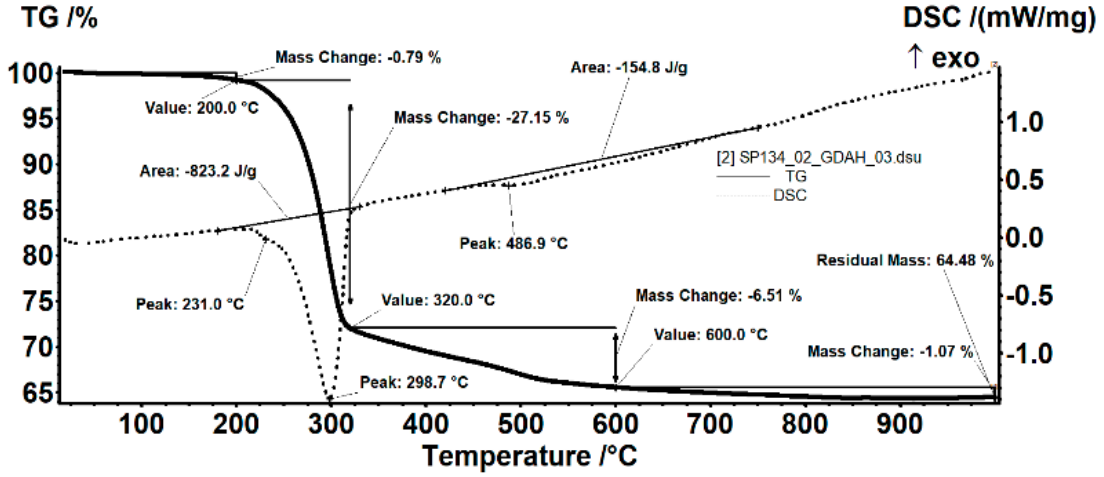

GDAH-03

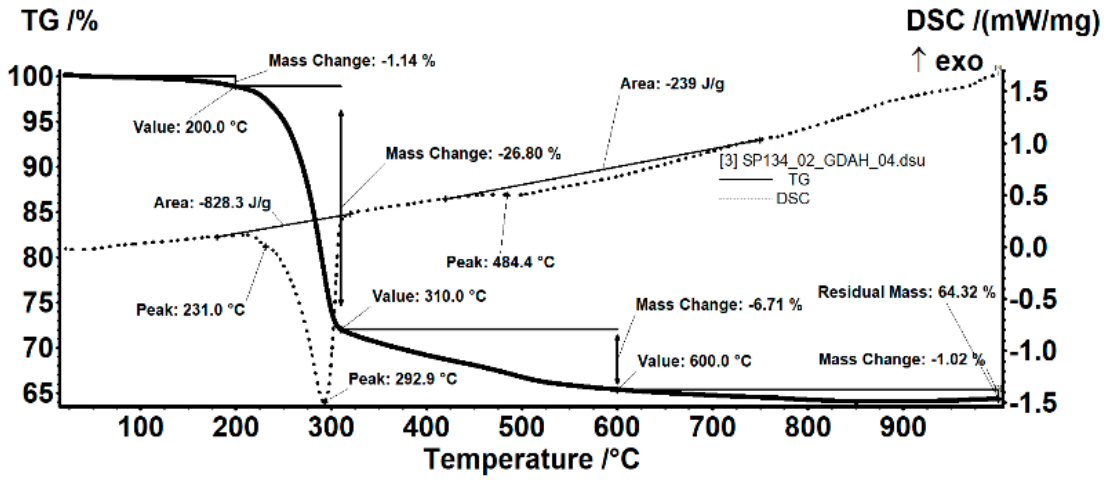

GDAH-04

Figure 1. *Cont.*

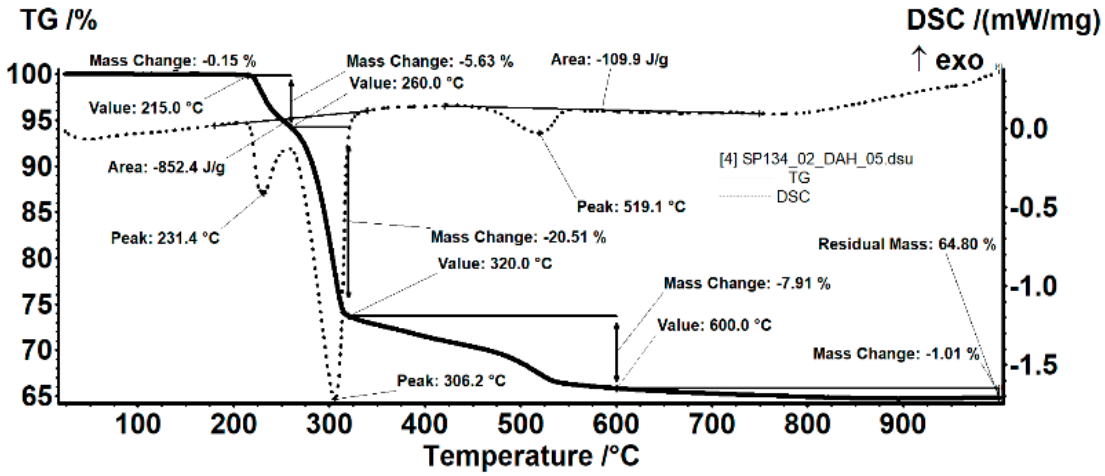

GDAH-05

Figure 1. TG and DSC curves of aluminum hydroxide powders heated at 10 °C/min.

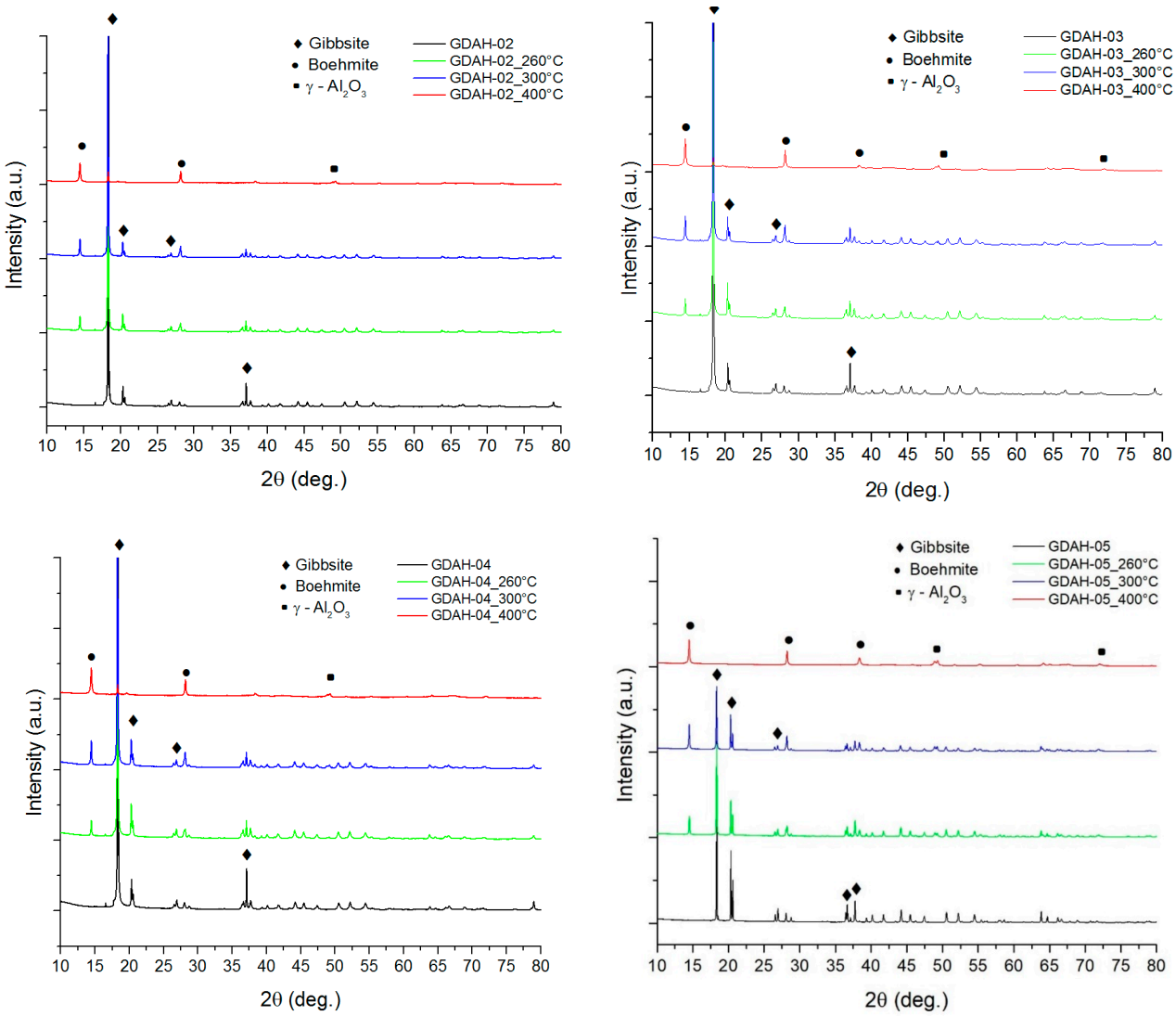

Figure 2. X-ray diffraction patterns for all samples.

Table 2. Effect of the calcination temperature on the phase composition and amorphous materials.

Sample	Mineral Name			Amorphous Phases (%)
	Gibbsite (%)	Boehmite (%)	γ-Al_2O_3 (%)	
GDAH-02	62.54	0.00	0.00	37.46
GDAH-02-260	46.42	4.15	0.00	49.43
GDAH-02-300	34.60	5.82	0.57	59.00
GDAH-02-400	3.32	7.45	10.61	78.60
GDAH-03	61.67	0.00	0.00	38.33
GDAH-03-260	45.41	2.80	0.00	51.79
GDAH-03-300	38.33	4.99	0.44	56.25
GDAH-03-400	0.05	5.44	12.81	81.70
GDAH-04	62.59	0.00	0.00	37.41
GDAH-04-260	53.23	2.62	0.00	44.15
GDAH-04-300	43.26	5.48	0.64	50.62
GDAH-04-400	2.28	6.86	12.98	77.88
GDAH	55.56	0.00	0.00	44.44
GDAH-05-260	43.48	8.28	0.00	48.24
GDAH-05-300	33.81	11.94	0.00	54.25
GDAH-05-400	0.05	12.86	13.79	73.32

In order to improve the extraction efficiency of alumina and to prevent boehmitic reversion, Alum SA Tulcea applies a modified technology for the processing of alumino-gibbsitic/goethitic bauxites. The major differences between this method and the standard procedure are: (1) the digestion temperature is raised from 100–110 °C to 140–145 °C in order to increase the reaction rate; and (2) the alkalinity of the Bayer caustic lye is increased by changing the factor $a_k = C(Na_2O)/C(Al_2O_3)$ from 1.35–1.45 to 1.75–1.85 in order to prevent boehmitic reversion [61,62]. The newly created conditions of a higher temperature and alkalinity make possible the homogeneous nucleation and growth of bayerite particles, which will later serve as germs for the precipitation and agglomeration of the gibbsite particles identified by the XRD analysis.

In agreement with the thermal analysis data, the Rietveld refinement results from Table 2 show an increase in boehmite content (%) when the temperature was raised simultaneously with a decrease in the sample's gibbsite content (%). The thermal treatment at 400 °C proved to be insufficient for the total transformation of the gibbsite to boehmite or any other crystalline phase, mainly in the case of small particle size samples. Furthermore, the highest amount of boehmite was observed in the case of the GDAH-05 sample at all calcination temperatures. This can be attributed to the same increased ability to retain water on the larger particles' surface, enabling boehmite formation, since GDAH-05 contains particles that are mostly between 45 and 100 µm in size [63]. Additionally, we observed that the crystallinity degree decreased as the thermal transformation temperature increased when the initial gibbsite phase was heated. Since a greater number of defects in the less-crystallized materials occurs very often in similar well-known experiments, a possible explanation might be the production of defects in the crystal at a high temperature, associated with a high degree of mobility at the atomic level when the gibbsite was calcined [38]. Literature studies consider the loss in crystallinity to be a result of the porous surface layer that forms when gibbsite is calcined in air. In these cases, the pore diameters shift with the temperature from 5 (170 °C) to 20 (500 °C) nm [64]. Moreover, from Table 2 it can be seen that up to 400 °C, neither of the two phase transitions mentioned above are fully finished, in accordance with the purpose of the experiment—to promote amorphous phase growth.

The particle size distribution and characteristic diameters (D10, D50, and D10) of the milled samples thermally treated at 260 °C, 300 °C, and 400 °C for 2 h are given in Figure 3. The variation in characteristic diameters with temperature indicates that the fine-grained particles have undergone aggregation and agglomeration processes during the thermal treatment, which leads to an increase in particle size [65].

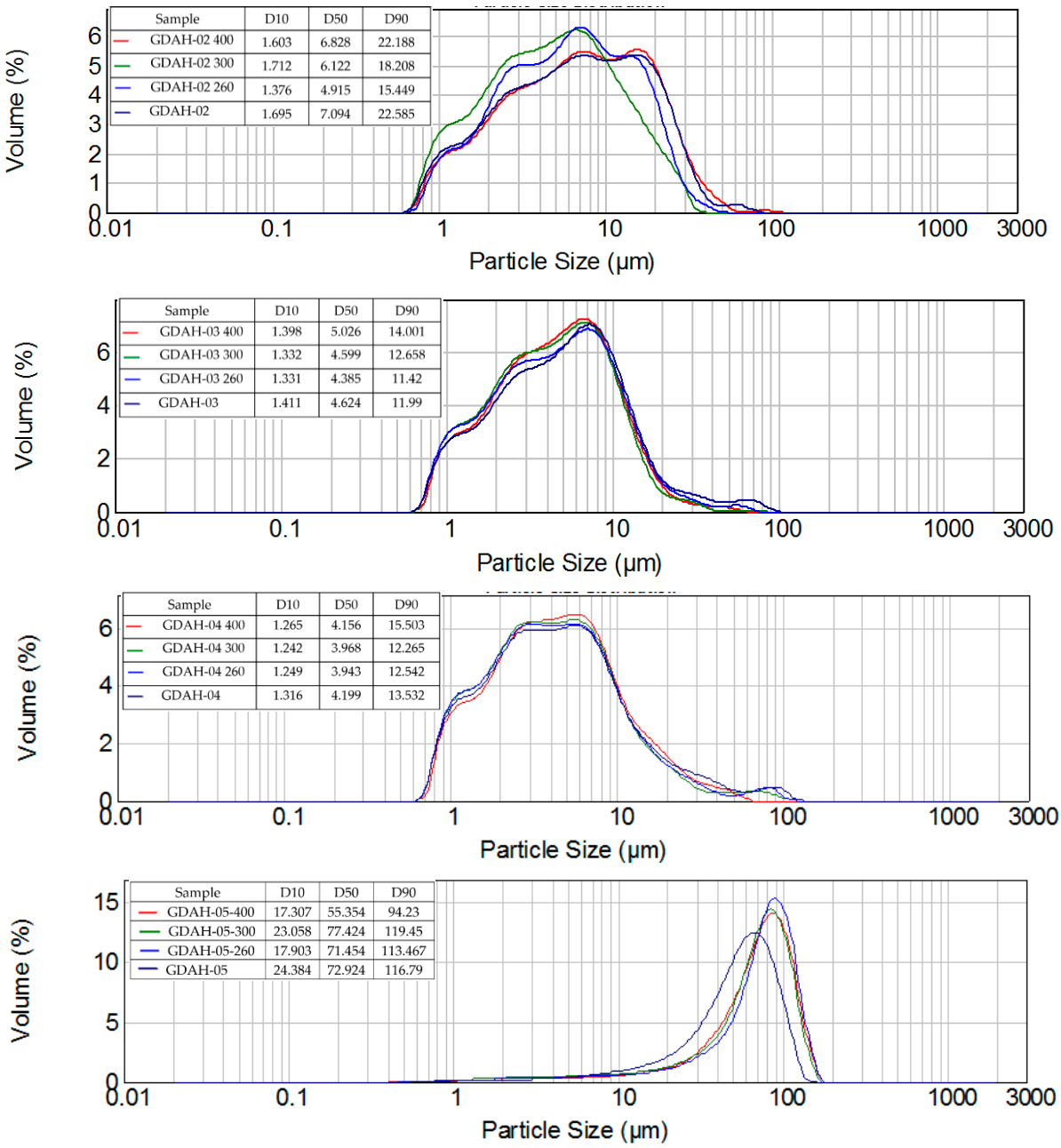

Figure 3. Particle size distributions for each powder, overlapped before and after calcination. The inserts show the D10, D50, and D90 numeric values for each sample before and after thermal treatment at 260 °C, 300 °C, and 400 °C.

In contrast, the GDAH-05 sample had a narrow particle size distribution when compared with the other products, with the median diameter D50 sharply reduced from around 70 µm before calcination to around 55 µm after calcination at 400 °C. The same phenomenon was identified also for the other characteristic diameters D10 and D90, in accordance with similar studies [64]. The thermal treatment triggered therefore a decrease in both the coarse and fine fractions of samples containing mostly large particles. The results can be correlated with previous studies on mechanically activated boehmite from the thermal decomposition of gibbsite [63,65].

All our results are in good agreement with best approaches to the subject found in the literature [66–72].

4. Conclusions

Aluminum hydroxide (gibbsite) samples with particle sizes between 10 and 150 µm were subjected to a thermal treatment in an electric furnace (in an air atmosphere) at 260 °C, 300 °C, and 400 °C for 2 h. At a temperature between ∼200 and 350 °C, the dehydroxylation of the gibbsite crystal lattice into the less-crystalline boehmite took place in two steps, with a considerable decrease in the phase transformation/transition temperature, when the particles sizes were significantly diminished. Additionally, the higher reactivity of the samples containing fine particles was displayed by a decrease in the AlOOH–γ-Al_2O_3 transformation/transition temperature. Calcination of the aluminum hydroxide samples produces, at a low temperature, a highly crystalline gibbsite phase, while at 400 °C a mixture of boehmite and γ-Al_2O_3 with a lower crystallinity degree was formed. Taken together, the experimental data suggest a strong correlation between the initial gibbsite particle size, the calcination temperature, the crystallinity degree, and the particle size distribution in the resulting aluminas calcined at low temperatures.

Author Contributions: Conceptualization, B.S.V. and L.F.; methodology, G.D., S.I. and L.C.; validation, A.B.; formal analysis, A.I.N.; investigation, V.A.S.; writing—original draft preparation, I.A.N.; writing—review and editing, I.A.N., B.S.V. and L.F.; visualization, A.I.N.; supervision, L.F.; project administration, B.S.V.; funding acquisition, B.S.V. All authors have read and agreed to the published version of the manuscript.

Funding: This research received no external funding.

Institutional Review Board Statement: Not applicable.

Informed Consent Statement: Not applicable.

Acknowledgments: This study was made possible by the implementation of the "Endow the Research and Development Department of SC ALUM SA Tulcea with independent and efficient research facilities to support the economic competitiveness and business development" project, co-funded by the European Regional Development Fund through the Competitiveness Operational Programme 2014–2020. Under this project were purchased and commissioned: "Independent equipment/installation for research and development of the technology of wet aluminum hydroxide classification", "Independent equipment/installation for research and development of technology to obtain the dried aluminum hydroxide", and "Independent equipment/installation for research and development of the technology of grinding and screening the dried aluminum hydroxide".

Conflicts of Interest: The authors declare no conflict of interest. The funders had no role in the design of the study; in the collection, analyses, or interpretation of data; in the writing of the manuscript; or in the decision to publish the results.

References

1. Meshcheryakov, E.; Kozlov, M.; Reshetnikov, S.; Isupova, L.; Livanova, A.; Kurzina, I. Studies of water-vapour adsorption dynamics of high-efficiency desiccant based on aluminium oxide and NaX zeolite. *Appl. Sci.* **2020**, *10*, 5320. [CrossRef]
2. Vivekh, P.; Ja, M.K.; Bui, D.; Chua, K. Recent developments in solid desiccant coated heat exchangers—A review. *Appl. Energy* **2018**, *229*, 778–803. [CrossRef]
3. Notorio Ribeiro, J.D.O.; Leite Vasconcelos, D.C.; Vasconcelos, W.L. Importance of the order of addition of the alumina precursor and its type into Al-SBA-15 mesoporous materials for use as water adsorbents. *Mater. Res.* **2019**, *22*, e20180651.
4. Le, T.H.; Nguyen, H.T. The Influence of Alumina Filler on Mechanical, Thermal and Electrical Properties of Bulk Moulding Compounds (BMCs) Composite. *Appl. Mech. Mater.* **2019**, *889*, 65–70. [CrossRef]
5. Saleh, M.; Al-Hajri, Z.; Popelka, A.; Zaidi, S.J. Preparation and characterization of alumina HDPE composites. *Materials* **2020**, *13*, 250. [CrossRef] [PubMed]
6. Chen, P.C.; Yang, L.C. Optimization and Characterization of Nano Aluminum Trihydrate-Based Flame-Retardant Materials in the Rotating Packed Bed Reactor. *Mater. Sci. Appl.* **2018**, *9*, 1036–1056. [CrossRef]
7. Hami, H.K.; Abbas, R.F.; Eltayef, E.M.; Mahdi, N.I. Mahdi Applications of aluminum oxide and nano aluminum oxide as adsorbents: Review. *Samarra J. Pure Appl. Sci.* **2020**, *2*, 19–32. [CrossRef]
8. Kim, J.; Lee, H.; Vo, H.T.; Lee, G.; Kim, N.; Jang, S.; Joo, J.B. Bead-shaped mesoporous alumina adsorbents for adsorption of ammonia. *Materials* **2020**, *13*, 1375. [CrossRef]
9. Szatyłowicz, E.; Skoczko, I. The use of activated alumina and magnetic field for the removal heavy metals from water. *J. Ecol. Eng.* **2018**, *19*, 61–67. [CrossRef]

10. Banerjee, S.; Dubey, S.; Gautam, R.K.; Chattopadhyaya, M.C.; Sharma, Y.C. Adsorption characteristics of alumina nano-particles for the removal of hazardous dye, Orange G from aqueous solutions. *Arab. J. Chem.* **2019**, *12*, 5339–5354. [CrossRef]
11. Norisetty, A.; Basu, J.K.; Sengupta, S. Application of Alumina to Oil and Grease Removal from Refinery Effluent. *Hydrol. Curr. Res.* **2011**, *2*, 100011. [CrossRef]
12. Li, W.; Franco, D.C.; Yang, M.S.; Zhu, X.; Zhang, H.; Shao, Y.; Zhang, H.; Zhu, J. Investigation of the Performance of ATH Powders in Organic Powder Coatings. *Coatings* **2019**, *9*, 110. [CrossRef]
13. Zhang, H.; Yang, B.; Yang, S.; Huang, J.; Cui, J.; Liu, W.; Shan, Y.; Zhang, H.; Zhu, J. Research Status and Development of Functional Powder Coatings, Chemcial Industry and Engineering. *Hydrol. Curr. Res.* **2020**, *37*, 1–18. [CrossRef]
14. Wang, Z.; Shen, X.; Yan, Y.; Qian, T.; Wang, J.; Sun, Q.; Jin, C. Facile fabrication of a PDMS @ stearic acid-$Al(OH)_3$ coating on lignocellulose composite with superhydrophobicity and flame retardancy. *Appl. Surf. Sci.* **2018**, *450*, 387–395. [CrossRef]
15. Souza, A.D.; Arruda, C.C.; Fernandes, L.; Antunes, M.L.; Kiyohara, P.K.; Salomão, R. Characterization of aluminum hy-droxide ($Al(OH)_3$) for use as a porogenic agent in castable ceramics. *J. Eur. Ceram. Soc.* **2015**, *35*, 803–812. [CrossRef]
16. Alexandrovich, I.; Sergeevna, E.; Buyakova, S.; Kulkov, S.N.; Viktorovich, R.; Mamontov, G.; Zhukov, I.A.; Dedova, E.S.; Levkov, R.V. Porous Ceramics Obtained with the Use of Aluminum Hydroxide Powder. *Orient. J. Chem.* **2016**, *32*, 93–100. [CrossRef]
17. Ali, M.S.; MA, A.; Tahir, S.M.; Jaafar, C.N.A.; Norkhairunnisa, M.; Matori, K.A. Preparation and characterization of porous alumina ceramics using different pore agents. *J. Ceram. Soc. Jpn.* **2017**, *125*, 402–412. [CrossRef]
18. Abyzov, A.M. Aluminum Oxide and Alumina Ceramics (review). Part 1. Properties of Al_2O_3 and Commercial Production of Dispersed Al_2O_3. *Refract. Ind. Ceram.* **2019**, *60*, 24–32. [CrossRef]
19. Abyzov, A.M. Aluminum Oxide and Alumina Ceramics (Review). Part 2. Foreign Manufacturers of Alumina Ceramics. Technologies and Research in the Field of Alumina Ceramics1. *Refract. Ind. Ceram.* **2019**, *60*, 33–42. [CrossRef]
20. Abyzov, A.M. Oxide and Alumina Ceramics (Review). Part 3. Russian Manufacturers of Alumina Ceramics1. *Refract. Ind. Ceram.* **2019**, *60*, 183–191. [CrossRef]
21. Amin, S.K.; Abdallah, H.A.M.; Roushdy, M.H.; El-Sherbiny, S.A. An overview of production and development of Ceramic Membranes. *Int. J. Appl. Eng. Res.* **2016**, *11*, 7708–7721.
22. Mouratib, R.; Achiou, B.; El Krati, M.; Younssi, S.A.; Tahiri, S. Low-cost ceramic membrane made from alumina and silica-rich water treatment sludge and its application to wastewater filtration. *J. Eur. Ceram. Soc.* **2020**, *40*, 594–5950. [CrossRef]
23. Hakami, M.W.; Alkhudhiri, A.; Al-Batty, S.; Zacharof, M.P.; Maddy, J.; Hilal, N. Ceramic Microfiltration Membranes in Wastewater Treatment: Filtration Behavior, Fouling and Prevention. *Membranes* **2020**, *10*, 248. [CrossRef] [PubMed]
24. Šereš, Z.; Maravić, N.; Takači, A.; Nikolić, I.; Šoronja-Simović, D.; Jokić, A.; Hodur, C. Treatment of vegetable oil refinery wastewater using alumina ceramic membrane: Optimization using response surface methodology. *J. Clean. Prod.* **2016**, *112*, 3132–3137. [CrossRef]
25. Busca, G. *Chapter Three—Structural, Surface, and Catalytic Properties of Aluminas, Advances in Catalysis*; Academic Press: Cambridge, MA, USA, 2014; Volume 57, pp. 319–404.
26. Busca, G. Silica-alumina catalytic materials: A critical review. *Catal. Today* **2019**, *357*, 621–629. [CrossRef]
27. Tregubenko, V.Y.; Belyi, A.S. Characterization of Acid-Modified Alumina as a Support for Reforming Catalysts. *Kinet. Catal.* **2020**, *61*, 130–136. [CrossRef]
28. Nikoofar, K.; Shahedi, Y.; Chenarboo, F.J. Nano Alumina Catalytic Applications in Organic Transformations. *Mini-Rev. Org. Chem.* **2019**, *16*, 102–110. [CrossRef]
29. Busca, G. The surface of transitional aluminas: A critical review. *Catal. Today* **2014**, *226*, 2–13. [CrossRef]
30. Wang, L.; Shi, C.; Wang, L.; Pan, L.; Zhang, X.; Zou, J. Rational design, synthesis, adsorption principles and applications of metaloxide adsorbents: A review. *Nanoscale* **2020**, *12*, 4790–4815. [CrossRef]
31. Kovarik, L.; Bowden, M.; Andersen, A.; Jaegers, N.R.; Washton, N.; Szanyi, J. Quantification of High Temperature Transition Al_2O_3 and Their Phase Transformations. *Angew. Chem.* **2020**, *59*, 21719–21727. [CrossRef]
32. Malki, A.; Mekhalif, Z.; Detriche, S.; Fonder, G.; Boumaza, A.; Djelloul, A. Calcination products of gibbsite studied by X-ray diffraction, XPS and solid-state NMR. *J. Solid State Chem.* **2014**, *215*, 8–15. [CrossRef]
33. Bruschi, L.; Mistura, G.; Nguyen, P.T.M.; Do, D.D.; Nicholson, D.; Park, S.-J.; Lee, W. Adsorption in alumina pores open at one and at both ends. *Nanoscale* **2014**, *7*, 2587–2596. [CrossRef] [PubMed]
34. Vo, H.T.; Kim, J.; Kim, N.Y.; Lee, J.K.; Joo, J.B. Effect of pore texture property of mesoporous alumina on adsorption performance of ammonia gas. *J. Ind. Eng. Chem.* **2020**, *91*, 129–138. [CrossRef]
35. Shirai, T.; Watanabe, H.; Fuji, M.; Takahashi, M. Structural Properties and Surface Characteristics on Aluminum Oxide Powders. *Annu. Rep. Ceram. Res. Lab. Nagoya Inst. Technol.* **2010**, *9*, 23–31.
36. Vieira Coelho, A.C.; Souza Santos, H.D.; Kiyohara, P.K.; Marcos, K.N.P.; Souza Santos, P.D. Surface Area, crystal morphology and characterization of transition alumina powders from a new gibbsite precursor. *Mater. Res.* **2007**, *10*, 183–189. [CrossRef]
37. Egorova, S.R.; Lamberov, A.A. Effect of the phase composition of gibbsite on the specific surface area of coarse Floccule of products formed in its dehydration under thermal treatment. *Russ. J. Appl. Chem.* **2014**, *87*, 1021–1030. [CrossRef]
38. Mehta, S.; Kalsotra, A.; Murat, M. A new approach to phase transformations in gibbsite: The role of the crystallinity. *Thermochim. Acta* **1992**, *205*, 191–203. [CrossRef]
39. Nortier, P.; Fourre, P.; Saad, A.M.; Saur, O.; Lavalley, J.C. Effects of crystallinity and morphology on the surface properties of alumina. *Appl. Catal.* **1990**, *61*, 141–160. [CrossRef]

40. Said, S.; Mikhail, S.; Riad, M. Recent processes for the production of alumina nano-particles. *Mater. Sci. Energy Technol.* **2020**, *3*, 344–363. [CrossRef]
41. Candela, L.; Perlmutter, D.D. Kinetics of boehmite formation by thermal decomposition of gibbsite. *Ind. Eng. Chem. Res.* **1992**, *31*, 694–700. [CrossRef]
42. Kim, H.-I.; Lee, S.K. Probing the transformation paths from aluminum (oxy)hydroxides (boehmite, bayerite, and gibbsite) to metastable alumina: A view from high-resolution 27Al MAS NMR. *Am. Miner.* **2021**, *106*, 389–403. [CrossRef]
43. Kloprogge, T.; Ruan, H.D.; Frost, R.L. Thermal decomposition of bauxite minerals: Infrared emission spectroscopy of gibbsite, boehmite and diaspore. *J. Mater. Sci.* **2002**, *37*, 1121–1129. [CrossRef]
44. Abdelkader, A.; Hussien, B.M.; Fawzy, E.M.; Ibrahim, A.A. Boehmite nanopowder recovered from aluminum cans waste as a potential adsorbent for the treatment of oilfield produced water. *Appl. Petrochem. Res.* **2021**, *11*, 137–146. [CrossRef]
45. Mohammadi, M.; Khodamorady, M.; Tahmasbi, B.; Bahrami, K.; Ghorbani-Choghamarani, A. Boehmite nanoparticles as versatile support for organic–inorganic hybrid materials: Synthesis, functionalization, and applications in eco-friendly catalysis. *J. Ind. Eng. Chem.* **2021**, *97*, 1–78. [CrossRef]
46. Dobra, G.; Iliev, S.; Cotet, L.; Boiangiu, A.; Hulka, I.; Kim, L.; Catrina, G.A.; Filipescu, L. Heavy Metals as Impurities in the Bayer Production Cycle of the Aluminum Hydroxide from Sierra Leone Bauxite. Preliminary Study. *J. Sib. Fed. Univ. Eng. Technol.* **2021**, 151–165. [CrossRef]
47. Dobra, G.; Garcia-Granda, S.; Iliev, S.; Cotet, L.; Iosif, H.; Negrea, P.; Duteanu, N.; Boiangiu, A.; Filipescu, L. Aluminum Hydroxide Impurities Occlusions and Contamination Sources. *Rev. Chim.* **2020**, *71*, 65–76. [CrossRef]
48. Landek, D.; Ćurković, L.; Gabelica, I.; Kerolli Mustafa, M.; Žmak, I. Optimization of Sintering Process of Alumina Ceramics Using Response Surface Methodology. *Sustainability* **2021**, *13*, 6739. [CrossRef]
49. Mercury, J.R.; Sucupira, J.; Rodríguez, M.A.; Cabral, A.; de Aza, A.H.; Pena, P. Influence of the milling conditions on the thermal decomposition of Bayer gibbsite. *Powder Technol.* **2020**, *362*, 188–196. [CrossRef]
50. Jang, S.-W.; Lee, H.-Y.; Lee, S.-M.; Shim, K.-B.; Lee, S.W. Mechanical activation effect on the transition of gibbsite to α-alumina. *J. Mater. Sci. Lett.* **2000**, *19*, 507–510. [CrossRef]
51. Tsuchida, T.; Ichikawa, N. Mechano-chemical phenomena of gibbsite, bayerite and boehmite by grinding. *React. Solids* **1989**, *7*, 207–217. [CrossRef]
52. Kano, J.; Saeki, S.; Saito, F.; Tanjo, M.; Yamazaki, S. Application of dry grinding to reduction in transformation temperature of aluminum hydroxides. *Int. J. Miner. Process.* **2000**, *60*, 91–100. [CrossRef]
53. Van Gog, H. First-principles study of dehydration interfaces between diaspore and corundum, gibbsite and boehmite, and boehmite and γ-Al_2O_3: Energetic stability, interface charge effects, and dehydration defects. *Appl. Surf. Sci.* **2021**, *541*, 148501. [CrossRef]
54. Brown, J.F.; Clark, D.; Elliott, W.W. 13. The thermal decomposition of the alumina trihydrate, gibbsite. *J. Chem. Soc.* **1953**, 84–88. [CrossRef]
55. Yamaguchi, G.; Sakamoto, K. Hydrothermal Reaction of Aluminumtrihydroxides. *Bull. Chem. Soc. Jpn.* **1959**, *32*, 696–699. [CrossRef]
56. Day, M.K.B.; Hill, V.J. Thermal Transformations of the Aluminas and their Hydrates. *Nature* **1952**, *170*, 539. [CrossRef]
57. Sato, T. Hydrothermal reaction of alumina trihydrate. *J. Appl. Chem.* **2007**, *10*, 414–417. [CrossRef]
58. Rouquerol, J.; Rouquerol, F.; Ganteaume, M. Thermal decomposition of gibbsite under low pressures. I. Formation of the boehmitic phase. *J. Catal.* **1975**, *36*, 99–110. [CrossRef]
59. Filho, R.W.N.D.; Rocha, G.D.A.; Montes, C.R.; Vieira-Coelho, A.C. Synthesis and Characterization of Boehmites Obtained from Gibbsite in Presence of Different Environments. *Mater. Res.* **2016**, *19*, 659–668. [CrossRef]
60. Woo, S.; Park, J.-H.; Rhee, C.K.; Lee, J.; Kim, H. Effect of thermal treatment on the aluminum hydroxide nanofibers synthesized by electrolysis of Al plates. *Microelectron. Eng.* **2012**, *89*, 89–91. [CrossRef]
61. Authier-Martin, M.; Forté, G.; Ostap, S.; See, J. The mineralogy of bauxite for producing smelter-grade alumina. *JOM* **2001**, *53*, 36–40. [CrossRef]
62. Matters, S. Reactions of lime under high temperature Bayer digestion conditions. In *10th International Alumina Quality Workshop*; AQW Incorporated: Walton, KY, USA, 2015; p. 373.
63. Baranyai, V.Z.; Kristály, F.; Szűcs, I. Influence of grain and crystallite size on the gibbsite to boehmite thermal transfor-mation. *Studia UBB Chem.* **2015**, *60*, 27–44.
64. Lopushan, V.I.; Kuznetsov, G.F.; Pletnev, R.N.; Kleshev, D.G. Kinetics of phase transitions of gibbsite during heat treatment in air and in water vapor. *Refract. Ind. Ceram.* **2007**, *48*, 378–382. [CrossRef]
65. Wang, Q.; Li, Y.; Li, S.; Chen, R.; Xiang, R.; Xu, N. Effects of particle size of $Al(OH)_3$ on the properties of porous purging materials. *J. Ceram. Soc. Jpn.* **2017**, *125*, 504–508. [CrossRef]
66. Gan, B.K.; Madsenb, I.C.; Hockridge, J.G. In situ X-ray diffraction of the transformation of gibbsite to a-alumina through calci-nation: Effect of particle size and heating rate. *J. Appl. Cryst.* **2009**, *42*, 697–705. [CrossRef]
67. Danilevich, V.V.; Klimov, O.; Nadeina, K.A.; Gerasimov, E.Y.; Cherepanova, S.V.; Vatutina, Y.V.; Noskov, A.S. Novel eco-friendly method for preparation of mesoporous alumina from the product of rapid thermal treatment of gibbsite. *Superlattices Microstruct.* **2018**, *120*, 148–160. [CrossRef]

68. Ibrahim, I.; Baharuddin, S.; Arbain, R.; Othman, A.; Joannes, C. Processing of local bauxite to obtain highly purified and fine alumina powder. In *International Conference of Sustainable Earth Resources Engineering 2020 IOP Conference Series: Earth and Environmental Science 641*; IOP Publishing: Bristol, UK, 2021. [CrossRef]
69. Redaoui, D.; Sahnoune, F.; Heraiz, M.; Raghdi, A. Mechanism and Kinetic Parameters of the Thermal Decomposition of Gibbsite $Al(OH)_3$ by Thermogravimetric Analysis. *Acta Phys. Pol. A* **2017**, *131*, 562–565. [CrossRef]
70. Gralik, G.; Chinelattot, A.L.; Chinelatto, A. Effect of different sources of alumina on the microstructure and mechanical properties of the triaxial porcelain. *Cerâmica* **2014**, *60*, 471–481. [CrossRef]
71. Vahidi, G.; Bajwa, D.S.; Shojaeiarani, J.; Stark, N.; Darabi, A. Advancements in traditional and nanosized flame retardants for polymers—A review. *J. Appl. Polym. Sci.* **2020**, *138*. [CrossRef]
72. Padilla, I.; López-Andrés, S.; López-Delgado, A. Effects of Different Raw Materials in the Synthesis of Boehmite and γ- and α-Alumina. *J. Chem.* **2016**, *2016*, 5353490. [CrossRef]